2021 IEEE/ASME International Conference on
Advanced Intelligent Mechatronics (AIM)

Gravity and Impedance Compensation of Body Weight Support System Driven by Two Series Elastic Actuators

Jihoo Kwak[1], Wiha Choi[2], *Student Member, IEEE*, Chan Lee[3], *Member, IEEE*, and Sehoon Oh[2], *Senior Member, IEEE*

***Abstract*—Robotic devices that can support a human's motions, such as exoskeletons, have recently drawn attention. Body weight support (BWS) systems are potential robotic devices that support and assist trunk motions with elaborate force control for rehabilitation and training exercises. This research presents a BWS system with two-dimensional motion assistance controlled by two series elastic actuators, which can perform not only weight compensation but also impedance compensation for trunk motion assistance.**

As the core technology of the proposed system, a wire-driven mechanism is developed that consists of a compact planetary-geared elastic actuator (cPEA), which is a series elastic actuator. All the dynamic aspects of the cPEA output torque, the tension-generating system using a winding drum, and the dynamics interacting with the BWS system are analyzed and used to design a motion assistive controller.

The functionality and ability of the proposed system are validated through experiments performed under various conditions. The results verify that the dynamic behavior of trunk motion can be assisted by the impedance control of the proposed BWS system. In particular, the inertial force required for the trunk motion can be reduced by the proposed BWS system.

I. Introduction

A. Background

In recent years, robots have been employed not only in industrial fields, but also for human–robot interactions. A typical example is the application of robots that interact with humans for rehabilitation and sports. By interacting with humans through an appropriate structure and control method, these robots can help humans have more diverse experiences and achieve better outcomes.

Several advanced robots have been developed to interact with a human's trunk motion when walking and exercising. Exoskeletons are the most well-known and popular examples of this type of robot. However, an exoskeleton is still a very complicated and expensive system, and the general public cannot easily access exoskeletons. Meanwhile, another system has been utilized to support a human's trunk in a simpler manner, that is, a body weight support (BWS) system, which lifts a human body using some mechanisms. This BWS system can be robotized for advanced weight support during various motions. For example, [1] introduced a robot that compensates for the constant force (i.e., weight), such that a patient can walk comfortably with less muscle activity.

An example of a robotized BWS system is ZeroG (Aretech®, Virginia) [2], which has been developed to support a person's exercising gait on actual ground. This system incorporates a lifting actuator installed on a linear rail such that a human can perform gait rehabilitation while his/her weight is compensated for with a constant force in the vertical direction.

KineAssist (KineAssist®, Illinois) is another widely utilized robotized BWS system designed to help maintain the balance of a patient with impaired balance [3], [4]. Such a mechanism can increase the stability of gait training and present the patient with a sense of stability.

In addition to weight compensation and balancing assistance, robotic instruments can use impedance control to provide the dynamic environmental forces required by a human for better exercise performance and entertainment. LOPES (Lower extremity Powered ExoSkeleton, University of Twente, Netherlands) employs impedance control in each joint, such that it can guide a human as well as follow his/her motions [5], [6].

To better assist trunk motions, GRAVITYASSIST (Sabanci University, Turkey) was proposed to provide compensation for the inertia and weight of a person. A unique feature of this robot is that it measures the acceleration of the upper body of a person, and the actuator generates a force that can compensate for the inertial force [7].

In the actuating mechanisms for these robotic devices, compliant wires have been considered for transmission instead of rigid links because of their flexibility. CAREX-7 (Columbia University, New York) utilized various wires to assist the upper limb movements with many degrees of freedom. A wire transmission mechanism is beneficial because it is light and provides force transmission in various directions [8], [9].

In addition, TruST (Columbia University, New York) was designed as a mechanism that supports the trunk of a person using four wires. This system allows a user to exercise the upper limbs with extensive assistance in the transverse plane [10].

This work was supported by the Korean government through the National Research Foundation (NRF-2019R1A2C2011444). (*Jihoo Kwak and Wiha Choi are co-first authors, and Sehoon Oh is the corresponding author.*)

[1] The author is with Flight Control Department, Korea Aerospace Industries, LTD, Sacheon, Republic of Korea. (e-mail: jihoo.kwak@koreaaero.com)

[2] The authors are with Department of Robotics Engineering, DGIST, Daegu, Republic of Korea. (e-mail: {choiwiha, sehoon}@dgist.ac.kr)

[3] The author is with Department of Robot Engineering, Yeungnam University, Gyeongsan, Republic of Korea (e-mail: chanlee2510@gmail.com)

978-1-6654-4139-1/21/$31.00 ©2021 IEEE

B. Required Technologies and the Contribution of This Research

The assistive forces provided by these devices help compensate for the weight and modulate the dynamic characteristics of human motion or environments to reduce the required human force for the motions. These different types of assistive forces are described as follows:

$$F_{assist}^{weight} = m^{w.c}g \text{ (weight compensation)} \quad (1)$$
$$F_{assist}^{imp} = m^{d.c}a \text{ (inertial force compensation)}, \quad (2)$$

where $m^{w.c}$ is the magnitude of the compensated weight; g is the gravity acceleration; a is the acceleration of the human; and $m^{d.c}$ is the mass reduction. Note that F_{assist}^{weight} in (1) is constant, whereas F_{assist}^{imp} in (2) dynamically changes based on the human's motion. In addition, F_{assist}^{imp} can be implemented utilizing impedance control [11]–[13] or admittance control [14]–[16], which has been widely employed in many robotic systems.

In addition to these compensating forces, lateral or rotational assistive force is required to attain balance in the frontal plane. The dynamic characteristics of the human gait in the frontal plane can be represented by the vertical motions influenced by the gravity and ground reaction force and the medio-lateral motions related to balance. That is, trunk motions can be analyzed in a two-dimensional manner; thus, the assistive forces (F_{assist}^{weight} and F_{assist}^{imp}) should be designed considering these degrees of freedom when creating a trunk motion assistive robot [17].

For this multi-dimensional motion assistance, many robots have adopted a wire transmission mechanism [1], [2], [8]–[10], [18], the tension of which is controlled to provide the desired forces. This adoption can be attributed to the advantages of wire transmission systems, namely low inertia, fewer constraints, and the degrees of freedom in the actuator location [8].

This paper proposes a novel trunk motion assistive body weight support system to satisfy the aforementioned requirements. The proposed BWS system is driven by two series elastic actuators (SEA) [19]–[22] such that the assistive force is controlled with high force tracking performance. The features of the proposed BWS system and the contributions of the paper are as follows.

1) A novel BWS system that is driven by two compact SEAs to provide high-performance assistive force generation is developed.
2) Gravity and impedance compensation algorithms are designed to assist a human's trunk motion. They can be utilized for various dynamic human activities such as virtual environment experiences, gait rehabilitation, and training exercises.
3) The proposed system provides two-dimensional compensation for the trunk motions in the frontal plane: vertical and rotational motions.
4) The effectiveness and performance of the proposed system and the algorithms are verified through experiments.

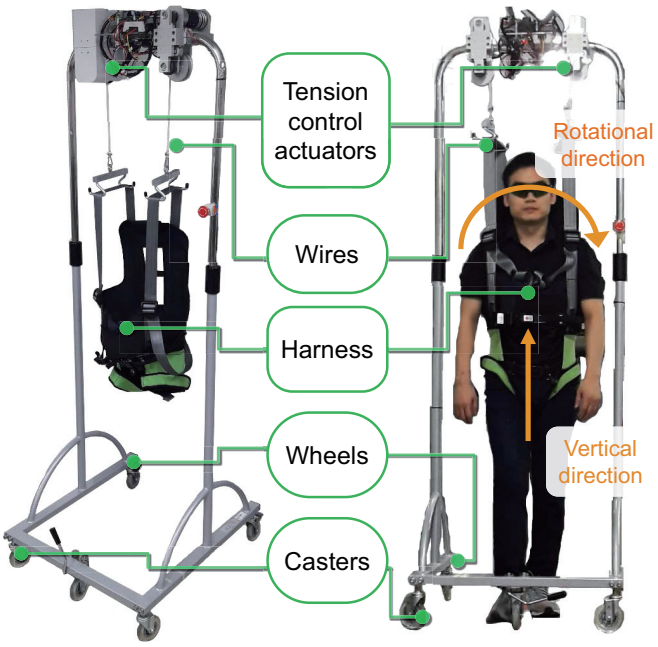

Fig. 1. Proposed BWS system for trunk motion assistance

II. SEA-DRIVEN TWO-DIMENSIONAL BWS SYSTEM

This section presents the configuration and concept of the proposed system.

A. Configuration of the Proposed BWS System

Fig. 1 presents an overview of the developed BWS system, which consists of two actuator systems, two wires, a harness, and four wheels, including two casters. The height of the frame can be adjusted according to the user's height—from 170 cm to 215 cm. A user wears a harness connected to two actuator systems through wires, as shown in Fig. 1. The trunk motion of the user is detected by the two actuator systems, which generate and transmit the desired interacting forces to the user through the wires and harness. Note that the actuator systems are connected on the right and left sides independently to provide two-dimensional assistive forces.

A compact planetary-geared elastic actuator (cPEA) [19], which is a Transmitted Force-sensing Series Elastic Actuator (TFSEA) [23], is employed as the actuator system. The details the cPEA are presented in Section II-B. The aim of the cPEA is to precisely detect the forces from the user and control the interacting force at high speeds. Table I summarizes the hardware specifications of the proposed system.

B. Wire Mechanism with Compact Planetary-geard Elastic Actuator

The interactive force of the proposed BWS system is provided through the wire mechanism, the tension of which is controlled by an SEA. Fig. 2 illustrates the wire mechanism equipped with a cPEA [24], a belt, and two pulleys. The cPEA in Fig. 3 was employed as the main actuator because it is compact and can generate a large force with high

TABLE I
SPECIFICATION OF THE PROPOSED BWS SYSTEM. THE ACTUATOR SPECIFICATION LISTED IS FOR A SINGLE ACTUATOR; TWO SUCH ACTUATORS ARE USED IN THE SYSTEM

Size	W: 73 cm D: 85 cm H: 170 - 215 cm
Radius of the wheel	10.5 cm
Diameter of the wire	5 mm
User weight (max. guaranteed)	100 kg
User weight (suggested)	Up to 80 kg
Vertical force (continuous)	598 N (61 kgf)
Vertical force (instantaneous)	1779 N (181 kgf)
Vertical velocity (continuous)	25.1 cm/s
Vertical velocity (instantaneous)	38.3 cm/s
Output power (continuous)	300 W
Output power (instantaneous)	1363 W
Motor	Maxon EC 4-pole 305015
Motor driver	Elmo Gold Solo Whistle 100/25
Control unit	NI myRIO-1900

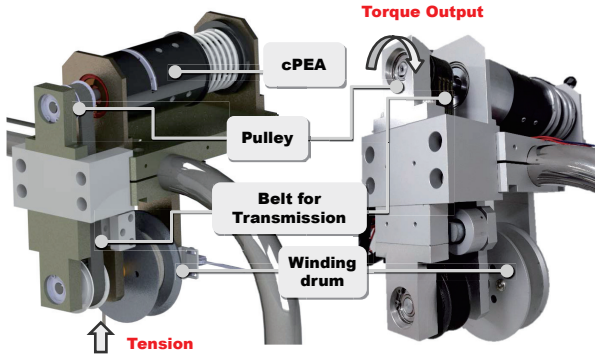

Fig. 2. Proposed wire mechanism equipped with series elastic actuator and winding drum

sensitivity [23]. The output torque of the cPEA in the proposed tension control actuator is transmitted to the winding drum through two pulleys, one belt, and the winding drum that lifts or releases the wire.

The wire tension is measured and controlled by the cPEA; however, the cPEA controls its torque, not the tension. Therefore, the relationship between the torque output of the cPEA τ_{out} and wire tension F must be derived. Wire tension F is also an intermediate control variable, and the trunk assistive force is the final target to be controlled. The relationship among these torques and forces is elaborated in Section III.

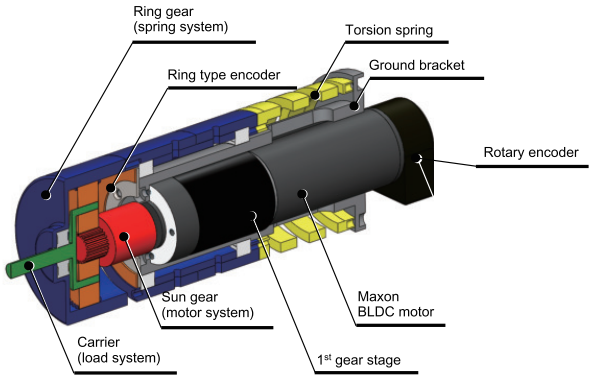

Fig. 3. Compact planetary-geared elastic actuator (from [24])

The specification of the actuator system was designed considering a human's trunk motion characteristics. The range of motion of the human trunk is 4 cm in the vertical direction and 7° in the roll direction [25]. Based on this, the range of the wire motion Δx was determined as follows:

$$\Delta x = \text{maximum vertical RoM} + \frac{\text{shoulder width}}{2} \times \text{maximum rotational RoM} \quad (3)$$

The diameter of the winding drum was determined to be 30 mm based on Δx, such that the fleet angle (which should be between $0.25°$ and $1.25°$ [26]) was not too large. A polyester wire with a diameter of 5 mm was employed.

III. TWO-DIMENSIONAL TRUNK MOTION ASSISTIVE CONTROL

This section describes in detail the control strategy and algorithms to achieve trunk motion assistance by using the proposed BWS system.

A. Wire Tension Control for Motion Assistive Control

Overall Control Configuration: Fig. 4 shows the overall control strategy of the proposed motion assistive control, where the two-phase control comprises trunk motion assistive control and wire tension control.

The trunk motion assistive control phase determines how much assistive force F_{ver}^{ref} and torque M_{rot}^{ref} should be provided in the vertical and rotational directions (*Trunk Motion Assistive Control* blocks in Fig. 4). The desired assistive forces are converted into the wire tension reference $F_{\{1,2\}}^{ref}$ based on the statics proposed in the following subsection (*Force Conversion* block in Fig. 4). The required wire tension reference is then realized by the high-performance control of the cPEA which can provide precise torques $\tau_{\{s1,s2\}}^{ref}$ (*Wire Tension Control* block in Fig. 4).

Force Transmission and Statics of the BWS System: To explain the proposed trunk motion assistive control, three types of forces/torques are discussed: 1) trunk assistive force F_{ver} and torque M_{rot}, 2) wire tensions F_1 and F_2, and 3) cPEA output torques τ_{out_1} and τ_{out_2}. The trunk force is designed to provide the desired assistive forces acting on the trunk motion as expressed in trunk motion space: F_{ver} is force in the vertical and M_{rot} is torque in the rotational direction in the frontal plane. The tensions F_1 and F_2 of the two wires interact with the human trunk to generate the trunk force. Finally, these tensions are controlled by two cPEA output torques τ_{out_1} and τ_{out_2}.

The statics of F_{ver}, M_{rot}, F_1, F_2, τ_{out_1} and τ_{out_2} are given as follows:

$$F_{ver} = F_1 + F_2 \quad (4)$$

$$M_{rot} = \frac{(F_1 - F_2) l_{app}}{2} \quad (5)$$

$$F_{\{1,2\}} = \frac{\tau_{\{out_1, out_2\}}}{R}, \quad (6)$$

where l_{app} is the shoulder width and R is the radius of the winding drum. The upper direction and the counterclockwise

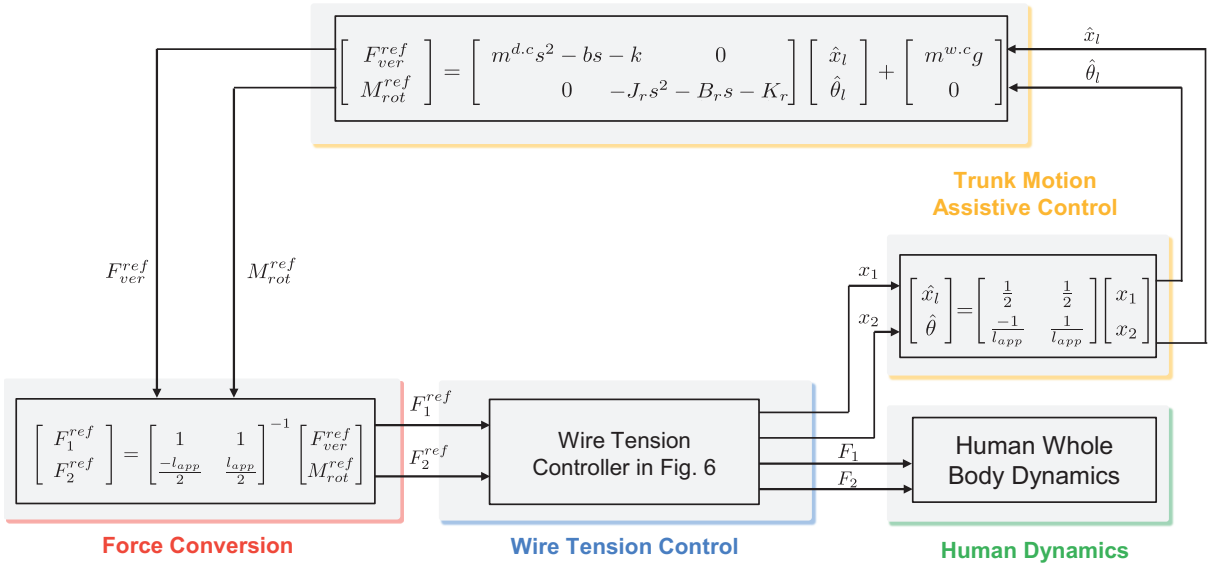

Fig. 4. Block diagram of the trunk motion assistive control configuration

direction are the positive directions for F_{ver} and M_{rot} in the remainder of the paper.

The reference transformation is conducted using the inverse of the statics in (4) and (5), which can be described as follows:

$$\begin{bmatrix} F_1^{ref} \\ F_2^{ref} \end{bmatrix} = \begin{bmatrix} 1 & 1 \\ \frac{-l_{app}}{2} & \frac{l_{app}}{2} \end{bmatrix}^{-1} \begin{bmatrix} F_{ver}^{ref} \\ M_{rot}^{ref} \end{bmatrix} \tag{7}$$

B. Motion Assistive Force Design using Impedance Control

As explained in Section I-B, the trunk assistive force is designed to reduce the loading caused by gravity (weight) and inertial force caused by motions. To understand the effectiveness of these forces, the dynamics of a human's center of mass (CoM) is formulated as follows:

$$m\ddot{x}_l + mg = F_{leg}, \tag{8}$$

where m is the mass of the human; F_{leg} is the human force in the vertical direction generated by the lower extremities; and $\ddot{x}_l$ is the vertical acceleration of the CoM. When the assistive forces in (1) and (2) are generated by the BWS system, the forces on the human change as follows:

$$\begin{aligned} m\ddot{x}_l + mg &= F_{leg} + F_{assist}^{weight} + F_{assist}^{imp}, \\ F_{leg} &= (m - m^{d.c})\ddot{x}_l + (m - m^{w.c})g \end{aligned} \tag{9}$$

The required force in (8), F_{leg} is reduced in (9) thanks to the assistive force that compensates for gravity and the inertial force.

Equation (9) is limited to the vertical direction, however, it can be extended to the rotational (roll) direction in the frontal plane. The modeling of the human dynamics in the roll direction is not as simple as it is in (8); however, it is clear that the lower extremity should generate a moment to retain the balance of the trunk in the rotational direction, which can be described as follows:

$$J\ddot{\theta} + M_{gvt} = M_{leg}, \tag{10}$$

where J is the moment of inertia of the trunk; M_{gvt} is the moment caused by gravity; and M_{leg} is the moment generated by the lower extremities. Note that, in general, the aim of M_{leg} is to suppress the effect of M_{gvt} not to generate the motion in θ. Regulation is important when it comes to the human dynamics in the rotational direction.

An assistive moment can help attenuate M_{leg} when it is properly designed. For example, an additional impedance $-J_r\ddot{\theta} - B_r\dot{\theta} - K_r\theta$ (additional inertial force and damping/stiffness generation in the rotational direction) to regulate the θ dynamics can reduce the M_{leg} required to maintain balance as follows:

$$\begin{aligned} J\ddot{\theta} + M_{gvt} &= M_{leg} - J_r\ddot{\theta} - B_r\dot{\theta} - K_r\theta \\ M_{leg} &= (J + J_r)\ddot{\theta} + B_r\dot{\theta} + K_r\theta + M_{gvt} \end{aligned} \tag{11}$$

The assistive forces in (1), (2), and (11) are designed for constant gravity compensation and dynamic motion assistive force. Dynamic motion assistive force can be realized utilizing impedance control, where the assistive force is designed using functions of the position, velocity, and acceleration. In summary, the proposed trunk motion assistive force design is given as follows:

$$\begin{bmatrix} F_{ver}^{ref} \\ M_{rot}^{ref} \end{bmatrix} = \begin{bmatrix} m^{d.c}\ddot{x}_l - b\dot{x}_l - kx_l + m^{w.c}g \\ -J_r\ddot{\theta} - B_r\dot{\theta} - K_r\hat{\theta} \end{bmatrix} \tag{12}$$

Compared with (1) and (2), the final assistive force design in (12) incorporates additional impedance characteristics (damping characteristics b and B_r as well as stiffness characteristics k and K_r) that can help reduce the required leg force and enhance stability.

Note that in this design, the vertical disposition parameters x_l and θ can be estimated from x_1 and x_2, which are wire length measurements. Equation (13) is the proposed estimation algorithm.

$$\begin{bmatrix} x_l \\ \theta \end{bmatrix} = \begin{bmatrix} \frac{1}{2} & \frac{1}{2} \\ \frac{-1}{l_{app}} & \frac{1}{l_{app}} \end{bmatrix} \begin{bmatrix} x_1 \\ x_2 \end{bmatrix} \tag{13}$$

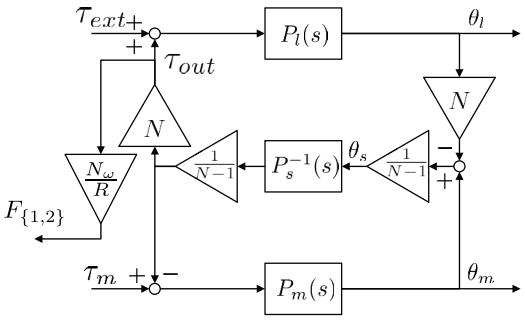

Fig. 5. Dynamic model of the wire tension mechanism with cPEA

The estimated x_l and θ are related to the trunk motion; thus, they can be utilized to detect abnormal trunk motions, such as falls. Safe ranges of x_l and θ are set to prevent these dangerous situations. The controller immediately switches to a position control mode and stops all the wire motions to guarantee the safety of the user when the motions of a person are outside this range.

C. Wire Tension Control of the Series Elastic Actuator

The wire tensions controlled by the cPEAs realize the desired trunk motion assistive force in (12). The statics in (7) converts the desired trunk assistive force (12) into the force references F_1^{ref} and F_2^{ref} for the two cPEAs. The control algorithm to precisely track the desired tensions F_1^{ref} and F_2^{ref} is discussed here.

Dynamic Modeling of the Wire Mechanism: The cPEA, which is the main force source of the proposed wire tension mechanism, can be modeled as shown in Fig. 5. In this figure, $P_m(s)$ is the motor dynamics; $P_s(s)$ is the spring dynamics; and $P_l(s)$ is the load dynamics [23], the transfer functions of which are given as follows:

$$P_m(s) = \frac{1}{J_m s^2 + B_m s} \quad (14)$$

$$P_s(s) = \frac{1}{J_s s^2 + B_s s + K_s} \quad (15)$$

$$P_l(s) = \frac{1}{J_l s^2 + B_l s} \quad (16)$$

Here, J_m, J_s and J_l are the values of the moment of inertia, and B_m, B_s and B_l are the damping values of the motor, the spring, and the load, respectively. Further K_s is the spring stiffness and τ_{out} is the output torque of the cPEA, which leads to the wire tension $F_{\{1,2\}}$, the relation of which is derived as follows:

$$F_{\{1,2\}} = \frac{N_w \tau_{out}}{R}, \quad (17)$$

where N_w represents the gear ratio of the belt–pulley structure and R represents the radius of the winding drum.

Hence, the transfer function from the motor torque to the wire tension is given as follows:

$$P_T = \frac{F_{\{1,2\}}(s)}{\tau_m(s)} = \frac{R^{-1} N_m^{-1} N_l N_w P_m}{N_m^{-2} P_m + N_l^2 P_l + (N_l - 1)^2 P_s}. \quad (18)$$

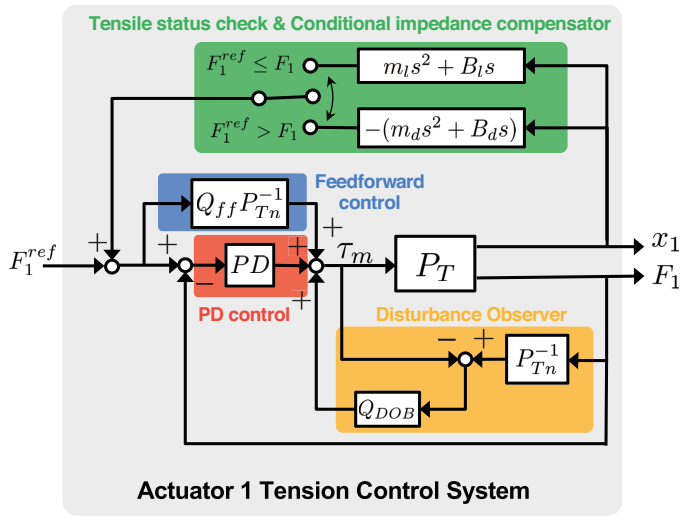

Fig. 6. Model-based Wire Tension Control Algorithm

TABLE II
PARAMETERS AND GAINS FOR WIRE TENSION CONTROL

K_t	0.0276 Nm/A	J_m	0.000004 kg·m^2
J_s	0.00048 kg·m^2	J_l	0.006 kg·m^2
B_m	0.000022 Nm·s/rad	B_s	0.8 Nm· s/rad
B_l	0.8 Nm· s/rad	K_s	39.52 Nm/rad
K_τ	0.0276 Nm/A	N_m	13.7959
N_l	9	N_w	28/18
R	0.03 m	$\tau_{Q_{DOB}}$	1/40π
$\tau_{Q_{ff}}$	1/20π	τ_{PD}	1/30π
K_P	2	K_D	0.2
m_d	0.003	m_l	0.002
B_d	0.04	B_l	0.22

Finally, the length of the wire $x_{\{1,2\}}$ is assumed to be $R\theta_{drum}$, which is a product of the drum radius R and the rotation angle θ_{drum} of the winding drum. The value of θ_{drum} is measured by an encoder.

Model-based Tension Controller: A model-based tension controller with a disturbance observer (DOB) [27], [28] is adopted to precisely control the wire tension. Figure. 6 illustrates the wire tension control algorithm consisting of the DOB, PD control, and feedforward controller.

The design of DOB was based on the model in (18). That is, the nominal model P_{Tn} in the DOB is modeled using (18). The parameters in (18) were identified using a CF-9400 FFT analyzer (ONO SOKKI®, Japan). In addition, Q_{DOB} is a second-order low-pass filter with the time constant set to $\tau_{Q_{DOB}}$. The feedforward controller utilizes the same identified P_{Tn} as its inverse form with a second-order low-pass filter Q_{ff} with time constant $\tau_{Q_{ff}}$. Table II shows all the parameters utilized in this research.

A conditional impedance compensator was added to keep the tension in the wire positive. When the desired tension is not properly generated with respect to the reference ($F_{\{1,2\}} < F_{\{1,2\}}^{ref}$), the winding drum is wound up as quickly as possible by the negative impedance ($-m_d\ddot{x}_{\{1,2\}} - B_d\dot{x}_{\{1,2\}}$). Meanwhile, a positive impedance ($m_l\ddot{x}_{\{1,2\}} + B_l\dot{x}_{\{1,2\}}$) is added when the wire tension is high enough ($F_{\{1,2\}} \ge F_{\{1,2\}}^{ref}$) to

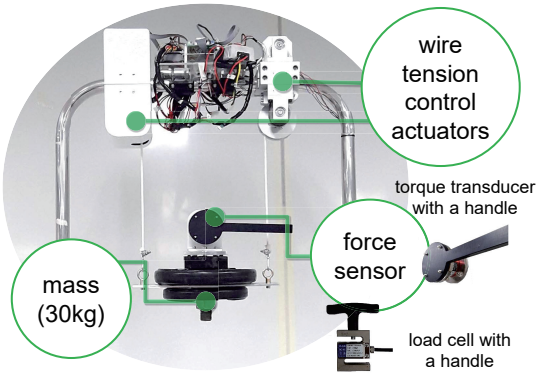

Fig. 7. Experimental set-up to evaluate the dynamic behavior of the proposed control actuators

prevent the tensile state from being released too quickly. The details of this compensator and its effectiveness were explained in our previous work.

IV. Verification of Trunk Motion Assistive Control through Experiments

The proposed trunk motion assistive control with the developed BWS was validated experimentally.

Two types of experiments were conducted. The dynamic behavior of the proposed BWS system under assistive control was first evaluated with a mass on the BWS system to investigate its dynamic behavior in a more controlled condition. Then, the effectiveness of the proposed assistive control was verified with a human wearing the BWS system.

A. Experiment on the Dynamic Behavior of the BWS System under Trunk Motion Assistive Control

The dynamic behavior of a mass attached on the BWS system was investigated to verify whether the assistive force was successfully realized in the proposed BWS system. Fig. 7 depicts a picture of the experimental setup for this, where a mass of 30 kg was attached at the end of the wires and the force/torque sensors were attached on top of the mass.

The assistive force realization must be validated in two stages. First, it is necessary to investigate whether the desired assistive force F_{ver}^{ref} and M_{rot}^{ref} is actually generated in the trunk space. Second, the actual relationship between $F_{ver}^{ref}, M_{rot}^{ref}$ and x_l, θ should be analyzed to verify whether the designed impedance in (12) is properly realized.

The accuracy of the trunk force generation, which is the first step, was investigated and reported in our previous work [29]. The realization of the impedance, which is the second step, is verified in this study. To this end, regulated external forces were applied to the mass on the BWS system, and its dynamic behavior was analyzed. Gravity was utilized (e.g., mg in (8) as the external force, and the trajectory of x_l during free fall was analyzed. The amount of this external force can be modulated by adding a gravity compensatory force $m^{w.c}g$ to F_{ver}^{ref} on top of the desired impedance.

Fig. 8 shows the experimental results, where the expected response of x_l from the simulation is represented by the dashed line, and the actual response obtained experimentally is represented by the solid line. The various impedance parameters in this experiment were initially set to the default settings $m^{d.c} = 0$ kg, $b = 70$ Ns/m, and $k = 475$ N/m. The external force was set to 5 kgf ($m^{w.c} = 25$).

Impedance sets with three values of each parameter were utilized. The trajectories of x_l were analyzed with regard to all the impedance sets. First, the trajectories with three different values of k (i.e., 475, 235, and 715) were measured and compared with the ideal trajectories (Fig. 8 (a)). Note that Coulomb friction was added in the simulations to account for the effect of nonlinear frictional forces on the timing belt, drum, and bearings.

The experimental and simulation results show that the steady-state value of x_l can be adjusted by setting the stiffness parameter k. In other words, a spring-like assistive force can be provided to the trunk by the proposed impedance control. Meanwhile, other behavioral characteristics, such as rising slope and damping characteristics, seem to remain the same because the other parameters $m^{d.c}$ and b were fixed values. The errors from the ideal trajectories are believed to be caused by the unmodeled non-linearities of transmission.

Fig. 8 (b) presents the pattern of response changes with different damping parameters (i.e., $b = 70$, 118, and 217). The transient aspects of the trajectories change with regard to the damping values: over-damped, critical damping, and small oscillatory behavioral characteristics are introduced by the proposed assistive force design. Note that the rising times remain almost the same because $m^{d.c}$ and k were fixed in all three cases.

Lastly, Fig. 8 (c) presents the response changes when the mass parameter changes (i.e., $m^{d.c} = -5, 0, 5$). The change in the rising slope is most evident in this case: the apparent weight $(30 - m^{d.c})$ decreases as $m^{d.c}$ increases; thus, the rising slope steepens.

Table III summarizes all experimental results. The responses of x_l in the experiments are quantitatively compared with the simulation results in terms of the rising time, settling time, and steady-state values.

The difference between the expected value and the measured value can be contributed to unmodelled nonlinearities in the mechanism. Fig. 2 shows the transmission mechanism between the torque output and the wire tension, which consists of two pulleys, one belt and one winding drum. These transmission mechanisms are subject to various nonlinearities such as friction and backlash, which can cause loss and difference in the relationships (4), (5), and (6).

The simulation result in Fig. 8 cannot fully model these nonlinearities, and thus the simulation cannot describe the actual measurements. However, the result still verifies that the proposed BWS system can control the dynamic behavior properly through impedance control.

The second experiment was conducted to evaluate rotational direction. Sets of various impedance values were set in the rotational direction by the proposed algorithm in (12). The rotational motion θ was then measured and analyzed when an additional step-wise input was applied. It is difficult to apply regulated torques precisely to the mass from the outside.

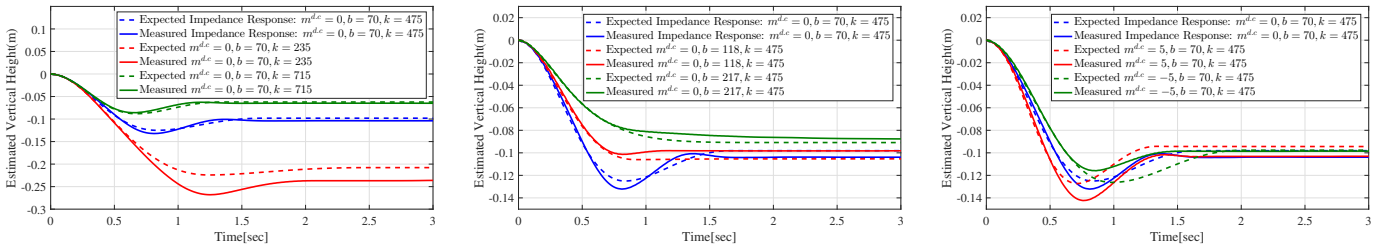

(a) Responses of various stiffness set-ups (b) Responses of various damping set-ups (c) Responses of various mass set-ups

Fig. 8. Step responses according to the varying impedance parameters in the vertical direction

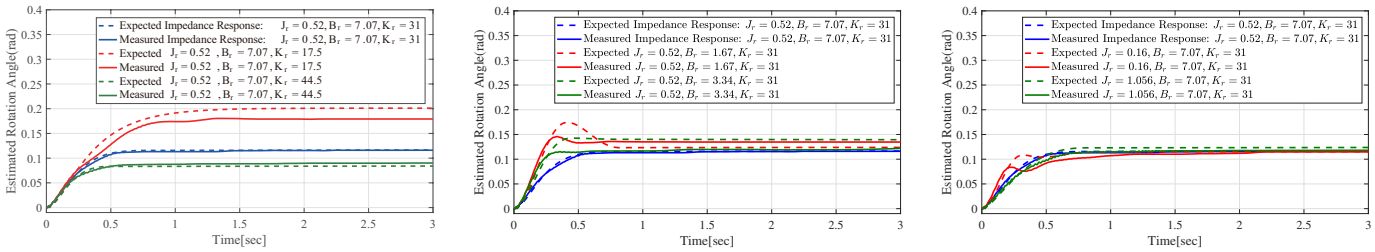

(a) Responses of various torsional stiffness set-ups (b) Responses of various torsional damping set-ups (c) Responses of the various moment of inertia set-ups

Fig. 9. Step responses according to varying impedance parameters in the rotational direction

TABLE III
STEP RESPONSE CHARACTERISTICS DESCRIBED IN FIG. 8. THE VERTICAL IMPEDANCE IS DESIGNED TO BE $(m-m^{d.c})\ddot{x_l}+b\dot{x_l}+kx_l$, WHERE THE ACTUAL MASS m IS SET TO 30. THE OTHER DEFAULT VIRTUAL IMPEDANCE PARAMETERS ARE SET TO $m^{d.c}=0, b=70$, AND $k=475$

Impedance	Response	Expected	Measured	Error(%)
Default	Rising time	0.360	0.386	7.173
	Settling time	1.49	1.20	19.38
	Steady-State	-0.0981	-0.104	6.014
$k=715$	Rising time	0.265	0.284	7.164
	Settling time	1.23	1.04	15.57
	Steady-state	-0.0622	-0.0648	4.180
$k=235$	Rising time	0.634	0.660	4.022
	Settling time	1.96	1.77	9.361
	Steady-state	-0.208	-0.237	13.94
$b=217$	Rising time	0.741	0.716	3.374
	Settling time	1.23	1.81	47.64
	Steady-state	-0.0909	-0.0876	3.576
$b=118$	Rising time	0.514	0.461	10.31
	Settling time	0.773	0.93	20.31
	Steady-state	-0.105	-0.0982	6.733
$m^{d.c}=-5$	Rising time	0.421	0.419	0.4751
	Settling time	1.811	1.316	27.33
	Steady-state	-0.0976	-0.0986	0.9731
$m^{d.c}=5$	Rising time	0.294	0.326	10.88
	Settling time	1.219	1.259	3.281
	Steady-state	-0.0944	-0.103	9.193

Hence, the external torque input (4 Nm) was emulated by the output torque of the cPEA.

Fig. 9 presents the experimental results, where the experimentally measured θ is represented by the solid lines, and the expected response calculated from the simulation is represented by the dashed lines. In a manner similar to that of x_l, rotation angle θ was estimated using (13) because its true value cannot be directly measured.

The default impedance setting was set to $J_r = 0.52$ kgm^2, $B_r = 7.07$ Nms/rad, and $K_r = 31$ Nm/rad. Fig. 9 (a) shows the response with different K_r values (31, 17.5, and 44.5), where the changes in the steady-state value of θ with regard to different K_r values can be confirmed. This is similar to result shown in Fig. 8 (a).

Fig. 9 (b) shows the response with different damping values ($B_r = 7.07$, 1.67, and 3.34), where the damping characteristics of the step response change with respect to the B_r setting. This result demonstrates that the damping of the trunk motion can be adjusted such that the balance in the frontal plane can be controlled by the proposed BWS system. The response in Fig. 9 (c) also shows a similar behavior to the result in Fig. 8 (c), where the rising slope changes with regard to the setting of J_r.

Overall, the proposed assistive control using the impedance in the rotational direction can properly change the dynamic behavior of the trunk, even though larger differences exist with respect to the theoretical behavior than do in the vertical motion case. The quantitative errors from the theoretical responses are listed in Table IV.

The impedance design for the trunk motion assistance of the proposed BWS was validated in another manner. The frequency characteristics of the BWS system were measured and compared with those of the theoretical one. The forces and torques were externally applied by a human, and the vertical x_l and rotational θ motions were measured. The frequency responses of $\frac{x_l}{F_{ext}}$, and $\frac{\theta}{M_{ext}}$ were then obtained from the experiments and compared with the desired response specified by the impedance design. The obtained frequency responses

TABLE IV
STEP RESPONSE CHARACTERISTICS OF THE RESULT PRESENTED IN FIG. 9. THE ROTATIONAL IMPEDANCE SET WAS $J_r\ddot{\theta} + B_r\dot{\theta} + K_r\theta$, AND THE PARAMETERS WERE SET TO $J_r = 0.52$, $B_r = 7.07$, AND $K_r = 31$

Impedance	Response	Expected	Measured	Error(%)
Default	Rising time	0.420	0.422	0.4762
	Settling time	0.626	1.41	125.4
	Steady-state	0.117	0.117	0.1715
$K_r = 44.5$	Rising time	0.265	0.410	54.72
	Settling time	0.426	1.162	172.8
	Steady-state	0.0841	0.0902	7.156
$K_r = 17.5$	Rising time	0.699	0.635	9.156
	Settling time	1.26	1.16	7.943
	Steady-state	0.201	0.179	10.89
$B_r = 3.34$	Rising time	0.246	0.231	6.098
	Settling time	0.542	2.719	401.7
	Steady-state	0.139	0.122	12.41
$B_r = 1.67$	Rising time	0.166	0.178	7.229
	Settling time	0.748	0.424	43.32
	Steady-state	0.124	0.135	8.717
$J_r = 1.056$	Rising time	0.512	0.516	0.7813
	Settling time	0.693	1.21	75.04
	Steady-state	0.124	0.118	4.685
$J_r = 0.16$	Rising time	0.634	0.793	25.08
	Settling time	0.761	2.07	171.6
	Steady-state	0.116	0.115	0.6920

are given as follows:

$$\frac{X_l(s)}{\mathcal{F}_{ext}} = \frac{1}{30s^2 + 70s + 475}$$
$$\frac{\Theta(s)}{\mathcal{M}_{ext}} = \frac{1}{0.52s^2 + 7.07s + 31} \tag{19}$$

$X_l, \mathcal{F}_{ext}, \Theta$, and $\mathcal{M}_{ext}$ are Laplace transforms of x_l, F_{ext}, θ, and M_{ext}, respectively.

The experiment was set up as shown in Fig. 7, where a load cell/torque sensor with a handle was fixed on the suspended mass. A person held the handle and generated the regulated sinusoidal forces/torques at frequencies of 0.25, 0.5, 0.75, 1, 1.5, and 2 Hz. The generated forces and torques were measured as F_{ext} and M_{ext}. The vertical motion x_l and rotating angle θ of the weight were obtained according to Eq. (13). The frequency response of the BWS was calculated by comparing the magnitude of each signal at each frequency. The experiments were performed three times for each frequency.

In the experiments, the impedance parameters for the vertical direction were set to the default values of $m^{d.c} = 0$ kg, $b = 70$ Ns/m, and $k = 475$ N/m. Meanwhile, for the rotation, they were set to $J_r = 0.52$ kgm^2, $B_r = 7.07$ Nms/rad, and $K_r = 31$ Nm/rad. Fig. 10 shows the experimental results.

The blue solid lines indicate the theoretical frequency response functions for the vertical and rotational directions, whereas the red circular points and bars are the means and the standard deviations, respectively, of the magnitudes of $\frac{x_l}{F_{ext}}$, and $\frac{\theta}{M_{ext}}$ calculated using the repeated experiments.

The measured frequency responses in Fig. 10 follow a similar behavior to the theoretical frequency response curves. Only the magnitude at 2 Hz in Fig. 10 (b) shows a large deviation. Considering the general frequency of human motion, a 2 Hz motion can be considered very fast [30], [31], and it is likely that the target frequency of the proposed BWS system should be set lower than this frequency. This frequency response result validates that assistive force can be applied to the human body by the BWS system to realize the desired frequency response.

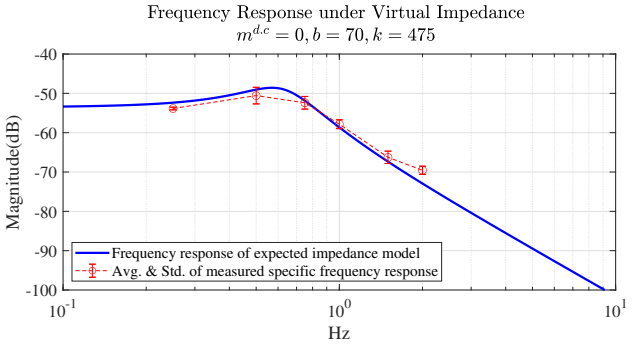

(a) Frequency response of the suspended mass along the vertical motion

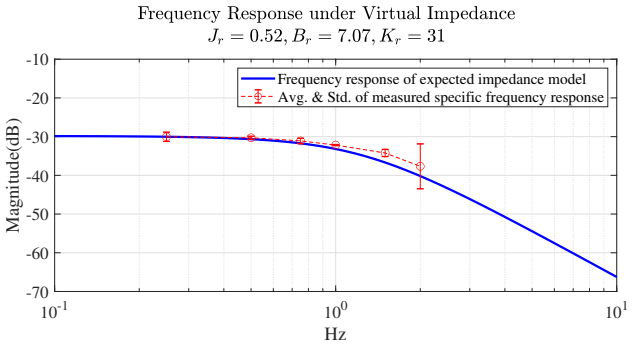

(b) Frequency response of the suspended mass along the rotational motion

Fig. 10. Frequency responses of the suspended mass to human hand interaction

B. Trunk Motion Assistance Experiments

The effectiveness of the proposed BWS system on the actual trunk motion was experimentally evaluated. To this end, a human's motion along with the proposed BWS system was measured and compared with the desired dynamic characteristics, which were calculated from a simplified model.

For the experiments, a subject wore a harness connected to the wire of the system with three markers attached to the center, left, and right regions of the pelvis for motion tracking. The subject stood on two force plates (AMTI®, Miami) to measure his/her weight and the changes in the ground reaction force. The Optitrack motion capture system (OptiTrack®, Oregon) was utilized for motion tracking.

In the first experiment, a subject (30-year-old male, 67 kg) wore the proposed BWS system and moved vertically with the designed assistive force acting on his body. The assistive force was designed to reduce 40% of the subject's weight ($m^{w.c} = 0.4 \times 67$ kg) as well as 40% of the inertial force ($m^{d.c} = 0.4 \times 67$ kg). The other impedance parameters in (12) were set to 0 ($b = 0, k = 0$) to verify whether the inertial force compensation worked well. The parameter settings were based on a preliminary study that found that the most comfortable movements are possible when the body weight compensation ratio and compensated inertia ratio are equal [7].

The subject repeated flexion and extension of the knee (squat posture) in accordance with the signal of a certain frequency. The theoretical inertial force was estimated based on the measured pelvis acceleration multiplied by the subject's mass. The ground reaction force during this motion was measured using two force plates and compared with the theoretical values. Two sets of vertical motions at frequencies of 0.5 Hz and 0.67 Hz were performed by the subject.

Fig. 11 represents the results of the comparison between the measured ground reaction force and the inertial force estimate. The blue solid line represents the measured force, whereas the red dashed line represents the calculated inertial force. Bias of up to $0.6 \times 67 \times 9.8$ N were subtracted from the measured values to focus on the inertial force characteristics; the blue line only illustrates the AC component of the force plate outputs.

Fig. 11 (a) shows the output with the 0.5 Hz motion, and (b) depicts the output with the 0.67 Hz motion. To compare two situations with and without 40% inertial assistance, the inertial force estimation was calculated using two different mass values: one estimation F^1_{inert} is with the original mass ($m = 67$ kg) and the other estimation $F^{0.6}_{inert}$ is with the compensated mass ($m = 0.6 \times 67$ kg), which are given as follows:

$$F^1_{inert} = m_{actual} \times \ddot{x}_{pelvis}, F^{0.6}_{inert} = 0.6 m_{actual} \times \ddot{x}_{pelvis}, \tag{20}$$

where m_{actual} represents the original mass of the subject and $\ddot{x}_{pelvis}$ represents the acceleration of the pelvis measured using OptiTrack. These two estimated values are depicted in Fig. 11 separately: the values of F^1_{inert} are shown in the upper graphs and the values of $F^{0.6}_{inert}$ are shown in the middle graphs.

Note that the measured vertical force matches well with the original mass estimation F^1_{inert} when the inertial force is negative (when the trunk goes down), whereas the measurements fit well with the reduced mass estimation $F^{0.6}_{inert}$ when the inertial force is positive (when trunk goes up) in both Fig. 11 (a) and (b). This result verifies that the inertial force of the trunk motion is successfully compensated by the proposed assistive device even though it affects the inertial force only in the upward direction, because the wire can only lift up the body, but not push it down. The lower graphs of Fig. 11 (a) and (b) are the measured GRF and the estimated inertial force without support, which shows that the inertial force is not compensated without support.

The differences between the inertial force estimation ($F^1_{inert}/F^{0.6}_{inert}$) and the ground reaction force (GRF) are compared using RMS (root mean square) values. The area for calculating the RMS difference is divided into two sections: the area where the GRF is positive and the area where the GRF is negative value. Based on this distinction, the RMS difference calculation was divided into four cases: Case 1 denotes the difference between the GRF and F^1_{inert}, when the GRF is positive, and Case 2 denotes the same difference calculation but when the GRF is negative. Case 3 denotes the difference between the GRF and $F^{0.6}_{inert}$ when the GRF is positive, and Case 4 is the same difference calculation but when the GRF is

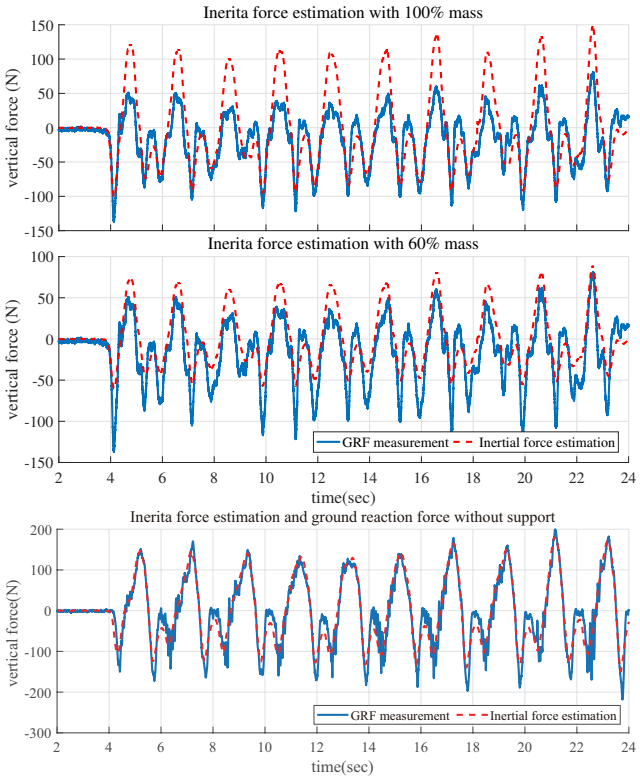

(a) Reaction force by the 0.5 Hz vertical motion

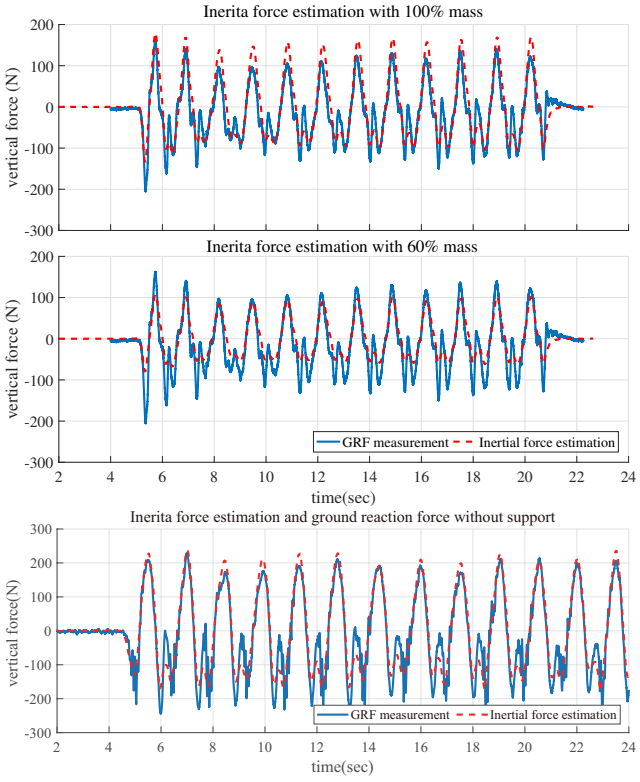

(b) Reaction force by the 0.67 Hz vertical motion

Fig. 11. Comparison of the measured ground reaction force and the inertial force estimation. The weight of the subject measured in the static state was subtracted such that only the inertial force can be measured. The subject repeated flexion and extension of the knee (squat posture) in accordance with the signal of a certain frequency. The assistive force was designed to reduce 40% of the subject's weight as well as 40 % of the inertial force.

TABLE V
COMPARISON OF THE RMS DIFFERENCES BETWEEN THE MEASURED GRF AND THE INERTIAL FORCE ESTIMATION

Motion Frequency	Case 1 F^1_{inert} (positive GRF)	Case 2 F^1_{inert} (negative GRF)	Case 3 $F^{0.6}_{inert}$ (positive GRF)	Case 4 $F^{0.6}_{inert}$ (negative GRF)
0.5 Hz	80.37	32.36	46.68	35.97
0.67 Hz	24.22	20.37	12.26	27.92

negative. The RMS values were calculated for these cases for both the 0.5 Hz and the 0.67 Hz experiments. The results are summarized in Table V. The results verify that $F^{0.6}_{inert}$ match better than F^1_{inert} in the positive GRF area (Case 3 is better than Case 1), and F^1_{inert} matches better than $F^{0.6}_{inert}$ in the negative GRF area. (Case 2 is better than Case 4).

The ability of the proposed BWS system to change the inertial force in the rotational direction was validated through another experiment. The subject flexed the left knee and the right knee alternately to generate rotational movements of the pelvis. The proposed BWS system was controlled to provide assistive moment with regard to this motion to retain balance. To this end, the impedance parameters in (12) were set to as $J_r = 0$ kg and $B_r = 0$ Nms/rad. Two values were used for K_r (40 and 80 Nm/rad) to investigate the functionality of the proposed assistive force design. Only weight compensation ($m^{w.c} = 0.4 \times 67$) was applied in the vertical direction during the rotation motion assistive control.

Similar to the vertical force comparison, the following torques in the rotational direction were calculated and compared with the measured values:

(1) *Torque calculated using the measured pelvis roll angle:* The angle of the pelvis motion in the roll direction was measured using motion capture and multiplied by the stiffness parameter ($K_r = 40,\ 80$ Nm/rad).

(2) *Torque measured using force plates:* The ground reaction forces were measured using the left and right force plates. The differences between the two values was calculated and multiplied by the half of the center-of-pressure (CoP) distance of the subject's feet.

Fig. 12 shows the comparison; the blue solid line represents the torque calculated from the motion capture, and the red dashed line represents the torque measured by the force plates. A high correspondence is found between the peaks in both cases even though the matches are not complete. This result implies that the rotational motion of the trunk can also be assisted as desired by the proposed BWS system.

The rotational motion assistance can help a person with hemiplegia retain their balance while walking. Additional experiments were conducted to verify this benefit, where a subject constrained his right leg, as shown in Fig. 13 (a), such that the knee and ankle joints could not rotate.

Three experiments were carried out: First, the subject walked without the constraint on his leg. The subject then walked with the right leg constrained and wore the BWS system; however, the impedance control was not applied. The reference for the assistive moment was set to zero so that the subject could generate the rotational motion freely.

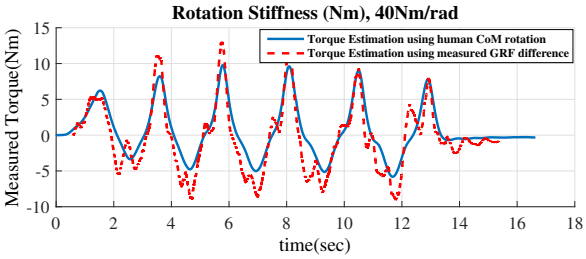

(a) One-side knee flexion motion (stiffness set to 40 Nm/rad)

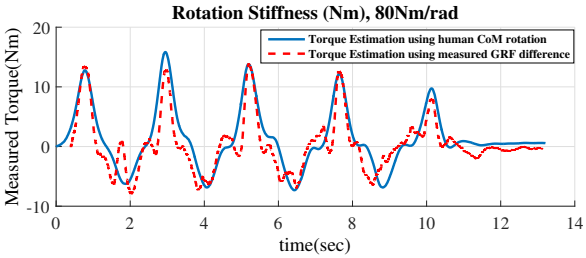

(b) One-side knee flexion motion (stiffness set to 80 Nm/rad)

Fig. 12. Comparison of the measured ground reaction torque and the inertial torque estimation

(a) Constrained leg

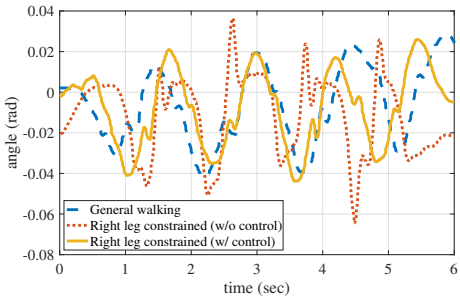

(b) Rotational motion trajectories

Fig. 13. Experimental set-up and results for asymmetric walking

Lastly, the subject walked with the constrained leg; however, the impedance control was applied to maintain his balance. The parameters for the impedance control were set as $B_r = 13$ Nms/rad and $K_r = 130$ Nm/rad. In all cases, the weight compensation in the vertical direction was applied with 10 kg weight compensation.

Fig. 13 (b) illustrates the results of the three cases and plots the rotational angles measured by two cPEAs. Of the three trajectories, the one with the constrained leg without impedance control shows the largest variation, whereas the other two show similar magnitudes.

The RMS values of the three trajectories were also calculated: the general walking obtained an RMS of 0.0171 rad, the constrained walking without control obtained an RMS of 0.0243 rad, and the constrained walking with control obtained an RMS of 0.0166 rad. These results demonstrate that the proposed BWS system with the rotational impedance control can help a human to regain the balance even when he/she has a disfunction in one leg.

V. Discussion and Conclusion

This study described a novel BWS system for trunk motion assistance. Its function and performance were validated through experiments. The proposed BWS system features a compact wire-driven mechanism with high performance tension control taking full advantage of a type of series elastic actuator, the cPEA. Thanks to the high-performance force controllability of the cPEA, elaborative trunk motion assistance can be performed by the proposed BWS. The performance of the whole system was validated through three sets of experiments: 1) time response verification and 2) frequency response verification using a mass as well as 3) the dynamic behavior of a human wearing the proposed BWS system.

The proposed trunk motion assistance incorporates an impedance control-type assistive force control design in addition to conventional constant body weight force compensation, which can help a human perform various motions by adjusting the dynamic force with regard to his/her motions. Through this control approach, a human can experience a light body or a different environment in which an artificial environmental force, such as damping or stiffness, supports their motion.

The experiments in Section IV scrutinized this feature by investigating the relationship between the vertical/rotational motions and the vertical force/rotational torque. The results show that the dynamic characteristics of a mass and a human can be controlled as desired by the proposed BWS system.

A dynamic force-controlled BWS system is not a new concept; however, the proposed BWS system is different from conventional dynamic BWS systems because 1) its assistance is two dimensional; 2) it provides an impedance control-based assistive force to attenuate inertial force and provide an artificial environmental force; and 3) it does not utilize any force sensors.

This research was conducted to examine the functional characteristics of the proposed BWS system, including human interactions. A clinical test focusing more on the human's motions is the future work of this research.

References

[1] M. Frey, G. Colombo, M. Vaglio, R. Bucher, M. Jorg, and R. Riener, "A novel mechatronic body weight support system," *IEEE Transactions on Neural Systems and Rehabilitation Engineering*, vol. 14, no. 3, pp. 311–321, 2006.

[2] D. Nichols, "Zerog: overground gait and balance training system," *Journal of rehabilitation research and development*, vol. 48, no. 4, p. 287, 2011.

[3] J. Patton, D. A. Brown, M. Peshkin, J. J. Santos-Munné, A. Makhlin, E. Lewis, E. J. Colgate, and D. Schwandt, "Kineassist: design and development of a robotic overground gait and balance therapy device," *Topics in stroke rehabilitation*, vol. 15, no. 2, pp. 131–139, 2008.

[4] M. Peshkin, D. A. Brown, J. J. Santos-Munné, A. Makhlin, E. Lewis, J. E. Colgate, J. Patton, and D. Schwandt, "Kineassist: A robotic overground gait and balance training device," in *Rehabilitation Robotics, 2005. ICORR 2005. 9th International Conference on*. IEEE, 2005, pp. 241–246.

[5] J. F. Veneman, R. Kruidhof, E. E. Hekman, R. Ekkelenkamp, E. H. Van Asseldonk, and H. Van Der Kooij, "Design and evaluation of the lopes exoskeleton robot for interactive gait rehabilitation," *IEEE Transactions on Neural Systems and Rehabilitation Engineering*, vol. 15, no. 3, pp. 379–386, 2007.

[6] H. van der Kooij, B. Koopman, and E. H. van Asseldonk, "Body weight support by virtual model control of an impedance controlled exoskeleton (lopes) for gait training." in *Engineering in Medicine and Biology Society, 2008. EMBS 2008. 30th Annual International Conference of the IEEE*. IEEE, 2008, pp. 1969–1972.

[7] H. Munawar and V. Patoglu, "Gravity-assist: A series elastic body weight support system with inertia compensation," in *Intelligent Robots and Systems (IROS), 2016 IEEE/RSJ International Conference on*. IEEE, 2016, pp. 3036–3041.

[8] X. Cui, W. Chen, X. Jin, and S. K. Agrawal, "Design of a 7-dof cable-driven arm exoskeleton (carex-7) and a controller for dexterous motion training or assistance," *IEEE/ASME Transactions on Mechatronics*, vol. 22, no. 1, pp. 161–172, 2017.

[9] Y. Mao and S. K. Agrawal, "Transition from mechanical arm to human arm with carex: A cable driven arm exoskeleton (carex) for neural rehabilitation," in *Robotics and Automation (ICRA), 2012 IEEE International Conference on*. IEEE, 2012, pp. 2457–2462.

[10] M. I. Khan, V. Santamaria, J. Kang, B. M. Bradley, J. P. Dutkowsky, A. M. Gordon, and S. K. Agrawal, "Enhancing seated stability using trunk support trainer (trust)," *IEEE Robotics and Automation Letters*, vol. 2, no. 3, pp. 1609–1616, 2017.

[11] S. Part, "Impedance control: An approach to manipulation," *Journal of dynamic systems, measurement, and control*, vol. 107, p. 17, 1985.

[12] C. Mitsantisuk, S. Katsura, and K. Ohishi, "Force control of human–robot interaction using twin direct-drive motor system based on modal space design," *IEEE Transactions on Industrial Electronics*, vol. 57, no. 4, pp. 1383–1392, 2010.

[13] K. Kong, "Proxy-based impedance control of a cable-driven assistive system," *Mechatronics*, vol. 23, no. 1, pp. 147–153, 2013.

[14] C. Ott, R. Mukherjee, and Y. Nakamura, "Unified impedance and admittance control," in *Robotics and Automation (ICRA), 2010 IEEE International Conference on*. IEEE, 2010, pp. 554–561.

[15] A. Lecours, B. Mayer-St-Onge, and C. Gosselin, "Variable admittance control of a four-degree-of-freedom intelligent assist device," in *Robotics and Automation (ICRA), 2012 IEEE International Conference on*. IEEE, 2012, pp. 3903–3908.

[16] P. Culmer, A. Jackson, M. Levesley, J. Savage, R. Richardson, J. Cozens, and B. Bhakta, "An admittance control scheme for a robotic upper-limb stroke rehabilitation system," in *Engineering in Medicine and Biology Society, 2005. IEEE-EMBS 2005. 27th Annual International Conference of the*. IEEE, 2006, pp. 5081–5084.

[17] C. Ott, *Cartesian impedance control of redundant and flexible-joint robots*. Springer, 2008.

[18] C. Lee and S. Oh, "Robust assistive force control of leg rehabilitation robot," in *2017 IEEE International Conference on Advanced Intelligent Mechatronics (AIM)*, July 2017, pp. 634–638.

[19] G. A. Pratt and M. M. Williamson, "Series elastic actuators," in *Intelligent Robots and Systems 95.'Human Robot Interaction and Cooperative Robots', Proceedings. 1995 IEEE/RSJ International Conference on*, vol. 1. IEEE, 1995, pp. 399–406.

[20] N. Paine, S. Oh, and L. Sentis, "Design and control considerations for high-performance series elastic actuators," *IEEE/ASME Transactions on Mechatronics*, vol. 19, no. 3, pp. 1080–1091, 2014.

[21] K. Kong, J. Bae, and M. Tomizuka, "A compact rotary series elastic actuator for human assistive systems," *IEEE/ASME transactions on mechatronics*, vol. 17, no. 2, pp. 288–297, 2012.

[22] P. Agarwal, Y. Yun, J. Fox, K. Madden, and A. D. Deshpande, "Design, control, and testing of a thumb exoskeleton with series elastic actuation," *The International Journal of Robotics Research*, vol. 36, no. 3, pp. 355–375, 2017.

[23] C. Lee, S. Kwak, J. Kwak, and S. Oh, "Generalization of series elastic actuator configurations and dynamic behavior comparison," *Actuators*, vol. 6, no. 3, 2017. [Online]. Available: http://www.mdpi.com/2076-0825/6/3/26

[24] C. Lee and S. Oh, "Configuration and performance analysis of a compact planetary geared elastic actuator," in *IECON 2016 - 42nd Annual Conference of the IEEE Industrial Electronics Society*, Oct 2016, pp. 6391–6396.

[25] A. Thorstensson, J. Nilsson, H. Carlson, and M. R. Zomlefer, "Trunk movements in human locomotion," *Acta Physiologica Scandinavica*, vol. 121, no. 1, pp. 9–22, 1984.

[26] C. Lee, J.-Y. Kim, S.-Y. Kim, and S. Oh, "Human force observation and assistance for lower limb rehabilitation using wire-driven series elastic actuator," *Mechatronics*, vol. 55, pp. 13 – 26, 2018. [Online]. Available: http://www.sciencedirect.com/science/article/pii/S0957415818301375

[27] S. Oh, C. Lee, and K. Kong, "Force control and force observer design of series elastic actuator based on its dynamic characteristics," in *Industrial*

Electronics Society, IECON 2015-41st Annual Conference of the IEEE. IEEE, 2015, pp. 004 639–004 644.

[28] S. Oh and K. Kong, "High-precision robust force control of a series elastic actuator," *IEEE/ASME Transactions on Mechatronics*, vol. 22, no. 1, pp. 71–80, Feb 2017.

[29] J. Kwak, W. Choi, and S. Oh, "Modal force and torque control with wire-tension control using series elastic actuator for body weight support system," in *IECON 2017 - 43rd Annual Conference of the IEEE Industrial Electronics Society*, Oct 2017, pp. 6739–6744.

[30] M. C. Morrissey, E. A. Harman, P. N. Frykman, and K. H. Han, "Early phase differential effects of slow and fast barbell squat training," *The American Journal of Sports Medicine*, vol. 26, no. 2, pp. 221–230, 1998, pMID: 9548115. [Online]. Available: https://doi.org/10.1177/03635465980260021101

[31] M. Spenko, H. Yu, and S. Dubowsky, "Robotic personal aids for mobility and monitoring for the elderly," *IEEE Transactions on Neural Systems and Rehabilitation Engineering*, vol. 14, no. 3, pp. 344–351, Sep. 2006.